

1
2
3
4
5
6
7
8
9
10
11
12
13
14
15
16
17
18
19
20
21
22
23
24
25

**Height correction of atmospheric motion vectors using satellite lidar
observations from CALIPSO**

Kathrin Folger and Martin Weissmann

Hans-Ertel-Centre for Weather Research, Data Assimilation Branch, Ludwig-Maximilians-
Universität, Munich, Germany

Manuscript for submission to the *Journal of Applied Meteorology and Climatology*

November 2013

Corresponding author address:

Kathrin Folger
LMU Meteorologie,
Theresienstraße 37,
80333 Munich, Germany
E-Mail: kathrin.folger@lmu.de

26 **Abstract**

27

28 Atmospheric Motion Vectors (AMVs) provide valuable wind information for the initial
29 conditions of numerical weather prediction models. However, height assignment issues and
30 horizontal error correlations require a rigid thinning of the available AMVs in current data
31 assimilation systems. The aim of this study is to investigate the feasibility of correcting the
32 pressure heights of operational AMVs from the geostationary satellites Meteosat-9 and
33 Meteosat-10 with cloud top heights derived from lidar observations by the polar orbiting
34 satellite CALIPSO. The study shows that the wind error of AMVs above 700 hPa is reduced
35 by 12-17% when AMV winds are assigned to 120 hPa deep layers below the lidar cloud tops.
36 This demonstrates the potential of lidar cloud observations for the improvement of the AMV
37 height assignment. In addition, the lidar correction reduces the slow bias of current upper
38 level AMVs and is expected to reduce the horizontal correlation of AMV errors.

39

40 **1. Introduction**

41

42 Observations from various geostationary and polar orbiting satellites are used to derive
43 Atmospheric Motion Vectors (AMVs) by tracking clouds or water vapor structures in
44 consecutive satellite images. AMVs provide outstanding global wind field coverage,
45 especially over oceans, where in-situ wind observations are rare. Wind observations are
46 particularly important for the initialization of numerical weather prediction (NWP) models
47 (Baker et al. 2013) and therefore, AMVs are an essential ingredient for NWP. The positive
48 impact of AMV assimilation in NWP models has been shown in several studies (e.g.
49 Bormann and Thépaut 2004; Velden et al. 2005). However, the vertical height assignment
50 remains a challenging task and introduces significant errors. These contribute up to 70% to

51 the total AMV error (Velden and Bedka 2009) and can be horizontally correlated over several
52 hundred kilometers (Bormann et al. 2003). Hence, AMVs are drastically thinned for the
53 assimilation in NWP models and only a small fraction of the available observations is used.
54 Preceding studies (Velden and Bedka 2009; Weissmann et al. 2013) demonstrated that AMVs
55 rather represent the wind in a vertically extended layer whereas they are traditionally
56 assimilated at discrete levels. In addition, Weissmann et al. (2013) showed that the height of
57 AMVs can be corrected using airborne lidar cloud top observations. The present paper further
58 investigates these two approaches that can potentially reduce the errors of AMVs. Firstly, we
59 treat AMVs as vertically extended layer observations instead of single level observations.
60 Secondly, satellite lidar cloud top observations are used to correct AMV pressure heights. The
61 paper is a follow-up study to Weissmann et al. (2013) where a small, regional sample of
62 airborne lidar observations was used as testbed for the AMV height correction with lidar
63 cloud top observations. As suggested in Weissmann et al. (2013), the present study conducts
64 the transition to larger scales using a sample of satellite lidar observations with significantly
65 larger size and longer temporal extent. Lidar cloud top height observations from the polar
66 orbiting satellite CALIPSO (Cloud-Aerosol Lidar and Infrared Pathfinder Satellite
67 Observations) are used to correct the heights of Meteosat-9 and Meteosat-10 AMVs. A
68 number of suitable vertical layers relative to the lidar cloud tops and relative to the original
69 AMV heights are investigated. Furthermore, different depths of the vertical layers are tested
70 to find an appropriate layer that should be assigned to AMVs in data assimilation systems.
71 Operational collocated radiosondes are used to validate AMV winds before and after the
72 height correction.

73

74

75

76 **2. Data and method**

77

78 **a. Data**

79

80 The present study comprises eight months (1 April - 6 October 2012 and 16 April - 13 June
81 2013) of operational AMVs that were derived hourly from the geostationary satellites
82 Meteosat-9 (2012 period) and Meteosat-10 (2013 period) by EUMETSAT (European
83 Organisation for the Exploitation of Meteorological Satellites). Both satellites are positioned
84 at 0° longitude and most of the height corrected AMVs are located over Europe and Africa,
85 where radiosondes are available for wind verification.

86 Meteosat AMVs from four different satellite channels are used: infra-red observations (IR) at
87 10.8 μm , visible observations (VIS) at 0.8 μm and observations from the water-vapor
88 channels (WV) at 6.2 μm and 7.3 μm . VIS-AMVs can only be tracked during daylight and are
89 derived for clouds in the lower troposphere, whereas IR-AMVs occur throughout the
90 troposphere and lower stratosphere. WV-AMVs from the two water vapour channels are
91 mainly positioned in the upper troposphere. The AMVs considered in this study are derived
92 by tracking cloud structures, whereas WV-AMVs tracking water-vapor structures in cloud-
93 free areas are excluded. The final AMV pressure height for Meteosat AMVs is determined by
94 different height assignment methods: IR-Window, IR/WV ratioing, H₂O intercept and the
95 CO₂-slicing technique (details in DiMichele et al. 2012). On 5 September 2012, the
96 EUMETSAT height assignment algorithm changed to the Cross-Correlation Contribution
97 (CCC) method (Borde and Oyama 2008). This method provides a more consistent height
98 assignment as the pixels that contribute most to the tracking process are used to set the AMV
99 height. However, the information about the specific height assignment method is no longer
100 available in the final data product.

101 Corresponding lidar cloud observations were obtained by the polar orbiting satellite
102 CALIPSO that was launched in 2006 and flies at an inclination of 98.2 degrees in a sun-
103 synchronous orbit at 705 km altitude. CALIPSO is part of the “A-Train”, which is a
104 constellation of several international science satellites that fly in formation and therefore
105 facilitate a wide variety of different observations of the same scenery from space. The lidar
106 CALIOP (Cloud-Aerosol Lidar with Orthogonal Polarization) aboard CALIPSO measures
107 vertical profiles of the atmospheric backscatter at two wavelengths (532 nm and 1064 nm),
108 which enables to determine the cloud top height with high horizontal and vertical resolution.
109 Additional measurements of the depolarization at 532 nm allow determining the cloud phase.
110 In this study, the official CALIPSO Level-2 cloud layer product is used. It provides inter alia
111 the 1-km horizontally averaged cloud top height from the CALIOP lidar, the number of
112 superimposed cloud layers, a quality index for clouds and the cloud phase. The vertical
113 resolution of the CALIOP lidar is 30 m at altitudes of -0.5 km to 8.2 km and 60 m from
114 8.2 km to 20.1 km (for more information on CALIPSO see Winker et al. 2009; Winker et al.
115 2010; Hunt et al. 2009). Missing CALIPSO observations on 27 days of the 8-month study
116 period lead to 220 days of available data.

117

118 **b. Collocation requirements**

119

120 AMVs are corrected with nearby CALIPSO lidar observations that are within 50 km
121 horizontal distance and 30 min time difference from the location and time of each AMV. The
122 median value of all available (at least 20) individual CALIPSO cloud top observations within
123 this range is taken as representative cloud top. In addition, the root mean square differences
124 between single lidar cloud observations and their median value must not exceed 70 hPa. All
125 multi-layer cloud scenes are discarded. The EUMETSAT AMV quality index (QI) must be

126 greater than 50, with 100 indicating the best possible value and 0 the worst. The quality index
127 for CALIPSO clouds also ranges from 0 (worst) to 100 (best) and has to exceed a value of 90.
128 In addition, the AMVs must be less than 100 hPa above and 200 hPa below the corresponding
129 CALIPSO cloud top height. This interval is chosen to account for the fact that lidar
130 observation and AMV may see different clouds due to the temporal and/or horizontal
131 displacement and based on the assumption that AMVs represent the wind below the actual
132 cloud top (Weissmann et al. 2013).

133 Figure 1 shows the position of Meteosat-9 AMVs and CALIPSO lidar observations on 1 April
134 2012 matching the described collocation requirements. For this day, we found 1247
135 collocated observations within the Meteosat-9 domain (approximately $\pm 63^\circ$ in each
136 direction from 0° longitude and 0° latitude). Typically, there are around 1000 -1300 Meteosat
137 AMVs per day that could be corrected with CALIPSO observations. Altogether, 243097
138 matches of Meteosat-AMVs and CALIPSO lidar observations are found in the complete
139 period of 220 days.

140 The AMV wind is evaluated using nearby operational radiosondes. As the wind field is
141 usually horizontally more uniform than cloud top heights, the collocation criterion for nearby
142 radiosondes is extended to 150 km and 90 min from the corresponding AMV. Thereby, both
143 the original AMV pressure height and the lidar cloud top height must be located at least
144 50 hPa below the highest level of the corresponding radiosonde. Given the comparably low
145 number of operational radiosondes, the sample size reduces to 4478 matches of Meteosat-
146 AMVs, CALIPSO lidar observations and operational radiosondes for the complete period.

147 The sample is divided into high-level AMVs with pressure heights < 300 hPa, mid-level AMVs
148 with pressure heights between 300 hPa and 700 hPa and low-level AMVs with pressure heights
149 ≥ 700 hPa. In total, 1259 high-level AMVs derived from the IR- and WV-channels (337 and 922
150 matches, respectively) are available. The respective CALIPSO observations are all classified
151 as ice clouds. The mid-level data set consists of 1576 AMVs (611 IR AMVs and 965 WV

152 AMVs) and the corresponding CALIPSO cloud products comprise 67% ice clouds and 33%
153 water clouds. The 1643 low-level AMVs from the IR- and VIS channels (219 and 1424
154 matches, respectively) are expected to correspond to water clouds only. Figure 2 shows the
155 vertical distribution of all AMVs that are used in this study.

156

157 **c. Height correction method**

158

159 The applied AMV height correction with satellite lidar observations from CALIPSO follows
160 Weissmann et al. (2013). AMV winds are compared to radiosonde winds vertically averaged
161 over layers of varying depth (0-200 hPa): firstly for layers relative to the originally assigned
162 AMV height and secondly for layers relative to the CALIPSO lidar cloud top height. If a layer
163 reaches the lowest or highest radiosonde level, the layer depth is reduced accordingly. Three
164 different layer positions are considered: (i) layers centered at the corresponding AMV height
165 or lidar cloud top height, (ii) layers with 25% above and 75% below the corresponding height
166 and (iii) layers from the corresponding height downward.

167

168 **3. Results**

169

170 **a. VRMS differences and wind speed bias**

171

172 Figure 3 shows the mean Vector Root Mean Square (VRMS) differences of AMVs and
173 radiosonde winds. These differences are calculated as the mean of the square-root of the sum of
174 the squared differences between AMV and layer-averaged radiosonde wind components u and v .
175 VRMS values are calculated for assigning AMVs to vertical layers of increasing depth, which are
176 computed by averaging radiosonde winds over the respective layer. The first set of layers uses the

177 original AMV height as reference (grey lines); the second set uses lidar cloud top observations as
178 reference (black lines). The corresponding wind speed bias is shown in Figure 4.

179 VRMS differences for high- and mid-level AMVs above 700 hPa (Fig. 3a – 3d) from WV-
180 and IR-channels exhibit a distinct error reduction when AMVs are treated as vertically
181 extended layers instead of as single level observations (which are the values for 0 hPa on the
182 x-axis). Lowest VRMS differences are achieved either by layers below the lidar cloud tops or
183 by layers with 25% above and 75% below the lidar cloud tops. The optimal depth of these
184 layers varies from 120 to 200 hPa. Layers below the lidar cloud tops exhibit lowest VRMS
185 differences for a depth of 100-150 hPa and layers with 25/75% above/below the lidar cloud
186 tops yield best results for a depth of 150-200 hPa. Overall, the shape of the curves for these
187 two lidar layers is fairly similar for the different subsets presented in Fig. 3a - 3d and small
188 differences in the position of the minimum may also be a result of the limited sample size of
189 individual subsets instead of systematic differences in between them. For all these four
190 subsets, the minimum of VRMS differences for layers relative to the lidar cloud top is in the
191 range of $0.5 - 1.5 \text{ m s}^{-1}$ lower than the lowest values reached with layers relative to the
192 original AMV height.

193 Figs. 4a and 4b exhibit a significant slow bias of high-level AMVs assigned to their original
194 discrete height (values for 0 hPa on the x-axis). Such a slow bias has also been found in other
195 recent studies (e.g. Bresky et al., 2012). Generally, the bias is reduced when AMVs are
196 assigned to deeper layers and results indicate that assigning them for example to layers of
197 100-150 hPa below the lidar cloud tops can also largely remove the slow bias of current upper
198 level AMVs. Overall, the results presented in Fig. 4 show that layers leading to low VRMS
199 differences tend to be similar to layers leading to a low wind speed bias.

200 In contrast to high- and mid-level AMVs, low-level AMVs (Figs. 3e and 3f) show a less
201 distinct benefit of incorporating lidar information. 200 hPa layers with 25/75% above/below
202 lidar cloud tops and 200 hPa layers below lidar cloud tops (for IR and VIS, respectively) lead

203 to the lowest VRMS differences, but results for layers of the same depth centered at the
204 original AMV heights are only 0.1-0.2 m s⁻¹ higher. As low-level AMVs are located at
205 pressure heights greater than 700 hPa, the 200 hPa layers below the lidar cloud top are mostly
206 layers from the lidar cloud tops to the lowest radiosonde level.

207 High- and mid-level AMVs overall exhibit a similar behavior and therefore all AMVs above
208 700 hPa are combined in Fig. 5. The combination of high- and mid-level AMVs will be
209 referred to as “upper-level AMVs” in the following. Results indicate that lowest VRMS
210 differences in combination with lowest wind speed bias values are achieved for either 120-
211 130 hPa layers below the lidar cloud tops or 200 hPa layers with 25/75% above/below the
212 lidar cloud tops.

213

214 **b. Relative VRMS reduction for lidar layers and lidar levels**

215

216 Figure 6 shows the relative reduction of VRMS differences when results for layers below the
217 lidar cloud tops are compared to results of layers of the same depth centered at the original
218 AMV heights (Fig. 6a) and results using the discrete original AMV heights (Fig. 6b). The
219 shape of the curves in Fig. 6a and 6b is similar. For upper level AMVs (black lines), best
220 results are yielded for layer depths of 100-120 hPa. Highest error reduction values are ~12%
221 for lidar layers compared to layers centered at the original AMV heights (Fig. 6a) and ~17%
222 compared to the discrete original AMV heights (Fig. 6b). The improvement is apparent in
223 both upper level channels IR and WV (black dotted and dashed lines). Dividing between
224 upper level ice clouds and water clouds leads to a similar error reduction and is therefore not
225 shown. Correcting the height of low-level AMVs (grey lines) with lidar information only
226 leads to a small error reduction, but the averaging over deep layers shows advantages over
227 using discrete heights.

228 After demonstrating the benefit of assigning AMVs to vertical layers below lidar cloud tops,
229 we now investigate how much of that error reduction could be achieved by assigning them to
230 one representative discrete level relative to the lidar cloud top instead. The black solid line in
231 Figure 7 represents the treatment of AMVs as a layer-average below the lidar cloud top
232 (equivalent to the black solid line in Figure 6b), whereas the dash-dotted line represents the
233 assignment of AMVs to the discrete mean pressure height of that lidar layer, i.e. a discrete
234 level located half of the layer depth below the lidar cloud top. Results indicate that assigning
235 AMVs to the mean pressure of the lidar layers achieves most of the reduction of assigning
236 AMVs to vertically extended lidar layers. However, interpreting AMVs as layer-averaged
237 winds leads to a relative reduction that is ~3% higher. The maximum of the curves is for both
238 approaches at ~120 hPa, which corresponds to using discrete levels 60 hPa below the lidar
239 cloud tops. The corresponding wind speed bias values at this maximum are for both
240 approaches close to zero (not shown).

241 Figure 8 illustrates the distribution of differences between the original AMV pressure and the
242 mean pressure level of 120 hPa deep layers below the lidar cloud top for upper level AMVs.
243 About 75% of the AMVs are located above the mean pressure of the lidar layers and are thus
244 shifted to lower altitudes (negative values) with the lidar height correction. As AMVs are
245 derived by tracking the motion of the cloud, the lidar cloud top (dashed line) marks the
246 natural upper edge where AMVs should be located. However, approximately 30% of the
247 AMVs are located above the cloud, which may be related to an erroneous height assignment
248 as well as to the temporal and horizontal displacement of AMV and CALIPSO lidar
249 observation. On average, upper level AMVs are located 31 hPa above the lidar layer center
250 (and correspondingly, 29 hPa below the lidar cloud top), with only small differences between
251 the single channels WV and IR. In summary, this indicates that the operational processing of
252 upper-level AMVs should consider that AMVs rather represent wind in a layer below the

253 actual cloud tops, but the systematic height differences are likely dependent on the applied
254 AMV processing systems and its settings.

255

256 **c. Effects of using different subsamples**

257

258 To investigate the effect of changes in the height assignment algorithm of EUMETSAT, the
259 analyzed 220 days are divided into three different time periods in Table 1. The first one
260 comprises 142 days before 5 September 2012, the day when the height assignment algorithm
261 was changed to the CCC-method. The second period consists of 32 days starting on
262 5 September 2012 and the last period consists of 46 days from 16 April until 12 June 2013.
263 According to the preceding results (see Fig. 6), the lidar layer depth is set to 120 hPa for
264 upper level AMVs and 200 hPa for low-level AMVs. For upper level AMVs, the error
265 reduction for assigning layers below the lidar cloud tops instead of the discrete original AMV
266 heights is apparent in all three periods ranging from 11.4% to 18.9%. As stated before, low-
267 level AMVs do not show a clear error reduction through the lidar height correction. However,
268 one noticeable feature is the high error reduction for low-level AMVs in the second period
269 from 5 September to 6 October 2012. This is likely related to a temporary degradation of the
270 quality of low-level AMVs in the time period after the height assignment algorithm changed
271 to the CCC-method (Salonen and Bormann 2012).

272 In order to utilize a reasonable large sample size, the collocation criterion for AMVs and
273 radiosondes in this study is set to 150 km and 90 minutes (see Section 2.2.). However, the
274 temporal and spatial displacement of AMVs and verification radiosondes introduces an
275 additional error component that is expected to be independent of the AMV error itself and the
276 height correction. Therefore, a weak collocation criterion leads to an underestimation of the
277 actual relative error reduction. Figure 9 shows how the relative error reduction for upper level
278 AMVs increases as the horizontal collocation criterion is tightened. Naturally, the number of

279 matches decreases for smaller distances. The error reduction for 120 hPa layers below the
280 lidar cloud tops relative to layers centered at the originally assigned AMV heights shows a
281 strong increase from ~12% at 150 km to ~21% at 40 km (black solid line). When compared to
282 the discrete original AMV height, the relative error reduction increases from ~17% to ~25%
283 (grey dashed line). Reducing the time difference does not lead to clearly larger improvements
284 and is therefore not shown.

285 This study uses a threshold for the AMV quality index QI of 50 (see section 2.2). Restricting
286 it to higher values (up to ≥ 80) reduces the sample size to up to ~60%. Table 2 lists the
287 relative error reduction for assigning 120 hPa layers (upper level AMVs) and 200 hPa layers
288 (low-level AMVs) below the lidar cloud tops instead of the discrete original AMV heights for
289 different quality thresholds. Restricting the sample to upper level AMVs with $QI \geq 80$ shows
290 slightly less improvement than including lower quality AMVs, but the differences are less
291 than 2.5%. For low-level AMVs, the error reduction slightly increases when only AMVs with
292 higher quality are regarded.

293

294 **4. Conclusion**

295

296 In this study, we use satellite lidar observations to correct the height of AMVs from Meteosat-
297 9 and Meteosat-10 with lidar cloud top observations from CALIPSO. 220 days of data with
298 altogether about 4500 collocated AMVs, CALIPSO observations and radiosondes are
299 analyzed. We investigate appropriate layer depths and layer positions relative to the lidar
300 cloud tops and relative to the original AMV heights by comparing AMV winds to radiosonde
301 winds averaged over layers of the respective depth and position.

302 For upper level AMVs, we found that assigning 120 hPa layers below the lidar cloud tops
303 leads to an improvement of ~12% compared to assigning layers of the same depth centered at
304 the original AMV heights and of ~17% compared to using the discrete original AMV heights.

305 Similar results are yielded for 200 hPa layers with 25% of the layer above and 75% below the
306 lidar cloud top. For AMVs above 700 hPa, the improvement is apparent in both channels and
307 both for ice and water clouds.

308 AMVs below 700 hPa only show a small error reduction when layers relative to the lidar
309 cloud tops are used instead of layers relative to the originally assigned AMV heights.
310 Although there is no clear error reduction for these AMVs using lidar information, there is
311 indication that lidar observations can reduce AMV errors in periods with lower AMV quality
312 due to changes in the AMV processing. The reasons why the lidar height correction is
313 showing much better results for upper level AMVs may be related to the fact that their wind
314 errors are generally larger.

315 A tighter threshold for the horizontal distance between AMVs and radiosondes used for
316 verification even leads to a clearly larger effect of the lidar height correction. The results
317 imply that the lidar height correction can actually reduce the AMV wind error by over 20%
318 compared to assigning AMVs to layers relative to the original heights and over 25%
319 compared to using the discrete original AMV heights, but the sample size gets comparably
320 small for a tight threshold.

321 Our results confirm the findings of preceding studies that AMVs are more representative of a
322 vertically extended layer wind instead of the wind at a discrete level (Velden and Bedka 2009;
323 Weissmann et al. 2013). Hernandez-Carrascal and Bormann (2013) showed in a simulated
324 framework that AMVs rather represent the wind within the cloud instead of the wind at the
325 cloud top or cloud base level. This is consistent with our finding that layers below the lidar
326 cloud tops yield best results. Alternatively, assigning AMVs to a level centered at the mean
327 pressure of the lidar cloud layer achieves most of the benefit of assigning AMVs to layers
328 below lidar cloud tops. This is also similar to the results of Hernandez-Carrascal and
329 Bormann (2013), where a discrete level at an adjusted pressure height can have similar effects
330 as a layer-averaged wind.

331 In summary, the results of this study demonstrate that the errors of Meteosat AMVs above
332 700 hPa can be significantly reduced when information from lidar cloud top observations is
333 incorporated. As already stated by other studies (Weissmann et al. 2013; Hernandez-Carrascal
334 and Bormann 2013), the best layer depth and layer position relative to the original AMV
335 height likely depends on the AMV processing and therefore varies from one data set to
336 another. Lidars in contrast, provide high-resolution cloud top observations that are expected to
337 be independent of the height assignment method used in the AMV processing. This implies
338 that the horizontal correlation of AMV errors can also be reduced.

339 The study uses a sample size of ~4500 collocated AMVs, CALIPSO observations and
340 radiosondes. The strongest restriction however, is the availability of radiosondes for
341 verification that are not required for the lidar height correction itself. Per day, there are about
342 1000-1300 Meteosat AMVs with nearby CALIPSO observations that could be directly
343 corrected with lidar information and it is assumed that the correction can also reduce the
344 errors of AMVs from other satellites.

345 Our study demonstrates the potential of using lidar cloud observations from CALIPSO or
346 other future space-based lidars for the height correction of AMVs. This suggests that NWP
347 may benefit from assimilating lidar-corrected AMVs and treating them as layer-averaged
348 AMVs in the future. However, even larger benefits for NWP may be achievable by using the
349 lidar information to develop situation-dependent quality control functions. In addition, lidar-
350 derived heights for AMVs could be used to validate different AMV processing algorithms.

351

352

353 **Acknowledgements**

354

355 The operational AMV and radiosonde data were provided by DWD (Deutscher Wetterdienst).

356 We would like to thank Alexander Cress and Harald Anlauf from DWD for helpful comments

357 and for the support with the data acquisition. The CALIPSO data were obtained from the
358 NASA Langley Research Center Atmospheric Science Data Center. We also thank Franziska
359 Schnell (LMU Munich) for her help with data access and Régis Borde (EUMETSAT) for
360 information on AMV height assignment. The study was carried out in the Hans-Ertel-Centre
361 for Weather Research. This German research network of universities, research institutes and
362 DWD is funded by the BMVBS (Federal Ministry of Transport, Building and Urban
363 Development).

364

365 **References**

366

367 Baker, W. E., R. Atlas, C. Cardinali, A. Clement, G. D. Emmitt, B. M. Gentry, R. M.
368 Hardesty, E. Källén, M. J. Kavaya, R. Langland, Z. Ma, M. Masutani, W. McCarty, R. B.
369 Pierce, Z. Pu, L. P. Riishojgaard, J. Ryan, S. Tucker, M. Weissmann, and J. G. Yoe, 2013:
370 Lidar-measured wind profiles – the missing link in the global observing system. *Bull. Amer.*
371 *Meteor. Soc.*, accepted, doi: 10.1175/BAMS-D-12-00164.1

372

373 Borde, R., and R. Oyama, 2008: A direct link between feature tracking and height assignment
374 of operational atmospheric motion vectors. *Proceedings of the 9th Int. Winds Workshop,*
375 *Annapolis, Maryland, USA, 14-18 April 2008 .*

376

377 Bormann, N., S. Saarinen, G. Kelly, and J.-N. Thépaut, 2003: The spatial structure of
378 observation errors in atmospheric motion vectors from geostationary satellite data. *Mon. Wea.*
379 *Rev.*, **131**, 706-718.

380

381 Bormann, N., and J.-N. Thépaut, 2004: Impact of MODIS polar winds in ECMWF's 4DVAR
382 data assimilation system. *Mon. Wea. Rev.*, **132**, 929-940.

383

384 Bresky, W. C., J. M. Daniels, A. A. Bailey, S. T. Wanzong, 2012: New methods toward
385 minimizing the slow speed bias associated with atmospheric motion vectors. *J. Appl. Meteor.*
386 *Climatol.*, **51**, 2137–2151.

387

388 Di Michele, S., T. McNally, P. Bauer, and I. Genkova, 2012: Quality assessment of cloud-top
389 height estimates from satellite IR radiances using the CALIPSO lidar. *IEEE Trans. Geosci.*
390 *Remote Sens.*, **51**, 2454-2464.

391

392 Hernandez-Carrascal, A., and N. Bormann, 2013, Atmospheric motion vectors from model
393 simulations. Part II: Interpretation as spatial and vertical averages of wind and role of clouds.
394 *J. Appl. Meteor. Climatol.*, accepted, doi: 10.1175/JAMC-D-12-0337.1

395

396 Hunt, W. H, D. M. Winker, M. A. Vaughan, K. A. Powell, P. L. Lucker, and C. Weimer,
397 2009: CALIPSO lidar description and performance assessment. *J. Atmos. Oceanic Technol.* ,
398 **26**, 1214-1228.

399

400 Salonen, K., and N. Bormann, 2012: Atmospheric motion vector observations in the ECMWF
401 system: Second year report, EUMETSAT/ECMWF fellowship programme research report
402 No.28.

403

404 Velden, C. S., J. Daniels, D. Stettner, D. Santek, J. Key, J. Dunion, K. Holmlund, G. Dengel,
405 W. Bresky, and P. Menzel, 2005: Recent innovations in deriving tropospheric winds from
406 meteorological satellites. *Bull. Amer. Meteor. Soc.* , **86**, 205-223.

407

408 Velden, C. S., and K. M. Bedka, 2009: Identifying the uncertainty in determining satellite-
409 derived atmospheric motion vector height attribution. *J. Appl. Meteor. Climatol.*, **48**, 450-463.

410

411 Weissmann, M., K. Folger, and H. Lange, 2013: Height correction of atmospheric motion
412 vectors using airborne lidar observations. *J. Appl. Meteor. Climatol.*, **52**, 1868–1877.

413

414 Winker, D. M., M. A. Vaughan, A. H. Omar, Y. Hu, K. A. Powell, Z. Liu, W. H. Hunt, and S.
415 A. Young, 2009: Overview of the CALIPSO mission and CALIOP data processing
416 algorithms. *J. Atmos. Oceanic Technol.*, **26**, 2310-2323.

417

418 Winker, D. M., J. Pelon, J. A. Coakley Jr., S. A. Ackerman, R. J. Charlson, P. R. Colarco, P.
419 Flamant, Q. Fu, R. M. Hoff, C. Kittaka, T. L. Kubar, H. Le Treut, M. P. McCormick, G.
420 Mégie, L. Poole, K. Powell, C. Trepte, M. A. Vaughan, B. A. Wielicki, 2010: The CALIPSO
421 mission: A global 3D view of aerosols and clouds. *Bull. Amer. Meteor. Soc.*, **91**, 1211–1229.

422

423

424

425

426

427

428

429

430

431

432

433

434 **TABLES**

435

		upper level AMVs		low level AMVs	
	time period	error reduction	counts	error reduction	counts
	All (220 days)	16.9	2835	7.1	1645
(1)	1 Apr. – 3 Sep. 2012 (142 days)	18.9	1725	5.1	999
(2)	5 Sep. – 6 Oct. 2012 (32 days)	11.4	406	18.5	249
(3)	16 Apr. – 12 June 2013 (46 days)	14.1	704	5.6	397

436

437

438 **TABLE 1.** Relative VRMS reduction in percent and number of matches for different time
 439 periods for assigning AMVs to layers below the lidar cloud tops instead of the discrete
 440 original AMV heights. The depth of the assigned layers is 120 hPa (200 hPa) for upper (low)
 441 level AMVs with pressure heights above (below) 700 hPa.

442

443

444

445

446

447

448

449

450

451

	upper level AMVs		low level AMVs	
QI	error reduction	matches	error reduction	matches
≥ 50	16.9	2835	7.1	1643
≥ 60	16.8	2573	8.0	1439
≥ 70	16.6	2265	8.3	1254
≥ 80	14.5	1792	9.4	1003

452

453

454 **TABLE 2.** Relative VRMS reduction in percent and number of matches for different quality
455 indices QI for assigning AMVs to layers below the lidar cloud tops instead of the discrete
456 original AMV heights. The layer depth is 120 hPa (200 hPa) for upper (low) level AMVs with
457 pressure heights above (below) 700 hPa.

458

459

460

461

462

463

464

465

466

467

468

469

470

471

472 **FIGURE CAPTIONS**

473

474 **FIG. 1.** Geographic position of 1247 collocated AMVs and CALIPSO lidar observations on
475 1 April 2012.

476

477 **FIG. 2.** Height distribution of all collocated AMVs and CALIPSO observations used in this
478 study.

479

480 **FIG 3.** Mean VRMS differences between AMV winds and layer-averaged radiosonde winds for
481 (a) high level IR-AMVs, (b) high level WV-AMVs, (c) mid level IR-AMVs, (d) mid level
482 WV-AMVs, (e) low level IR-AMVs and (f) low level VIS-AMVs. Numbers in brackets are
483 AMV counts for the respective graph. Grey lines represent layers relative to the original
484 AMV pressure height, black lines relative to the lidar cloud top height. The three different
485 layer positions are indicated by different line styles (cf. legend).

486

487 **FIG. 4.** As in Fig. 3 but for wind speed bias. Grey lines represent layers relative to the
488 original AMV pressure height, black lines relative to the lidar cloud top height.

489

490 **FIG. 5.** Mean VRMS and wind speed bias of differences between AMV winds and layer-
491 averaged radiosonde winds for upper level AMVs above 700 hPa (IR and WV combined).
492 Altogether, 2835 AMVs are used (948 IR and 1887 WV). Grey lines represent layers relative
493 to the original AMV pressure height, black lines relative to the lidar cloud top height. Note
494 that the scales for bias and mean VRMS values are different.

495

496 **FIG. 6.** Relative reduction of VRMS differences between AMV and radiosonde winds for
497 assigning AMVs to layers below the lidar cloud tops instead of (a) layers of the same depth

498 centered at the original AMV heights and (b) the discrete original AMV heights. Upper level
499 AMVs above 700 hPa (black solid line) are additionally divided into upper level WV-AMVs
500 (black dotted) and upper level IR-AMVs (black dashed). The grey solid line represents results for
501 lower level AMVs (≥ 700 hPa).

502

503 **FIG. 7.** Relative reduction of VRMS differences between AMV and radiosonde winds for
504 assigning AMVs to layers below the lidar cloud tops (solid line) and to the respective mean
505 pressure levels of that layer below lidar cloud tops (dashed-dotted line) instead of the discrete
506 original AMV heights.

507

508 **FIG. 8.** Histogram of height differences (hPa) between the original AMV pressure height and
509 the mean pressure of the corresponding 120 hPa layers below the lidar cloud top for upper
510 level AMVs above 700 hPa (1887 WV-AMVs and 948 IR-AMVs). The dashed vertical line
511 corresponds to the pressure height of the lidar cloud top.

512

513 **FIG. 9.** Relative VRMS reduction of differences between AMV and radiosonde winds as a
514 function of their horizontal distance for assigning AMVs to 120 hPa layers below the lidar
515 cloud tops instead of layers centered at the original AMV heights (solid line) and the original
516 discrete AMV heights (dashed line). The dotted line corresponds to the y-axis-label on the right
517 and shows the sample size.

518

519

520

521

522

523

FIGURES

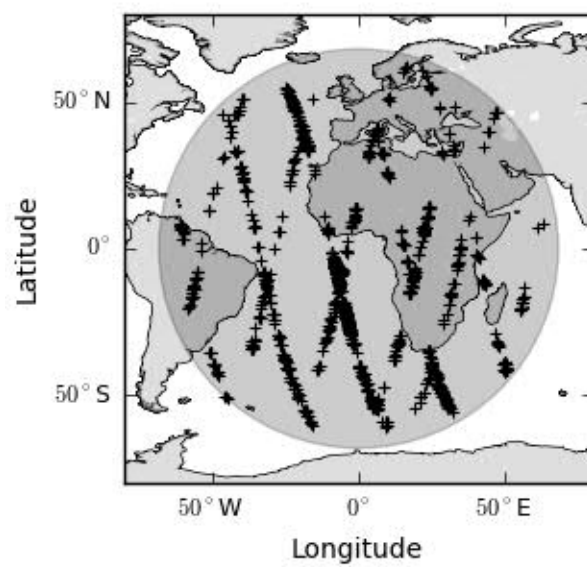


FIG. 1. Geographic position of 1247 collocated AMVs and CALIPSO lidar observations on 1 April 2012.

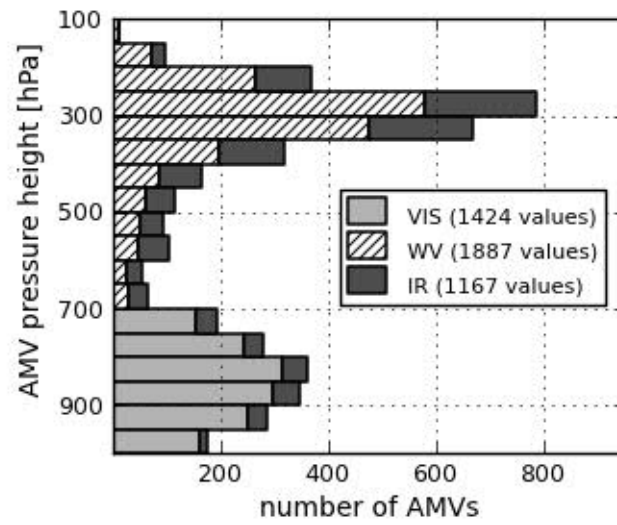


FIG. 2. Height distribution of all collocated AMVs and CALIPSO observations used in this study.

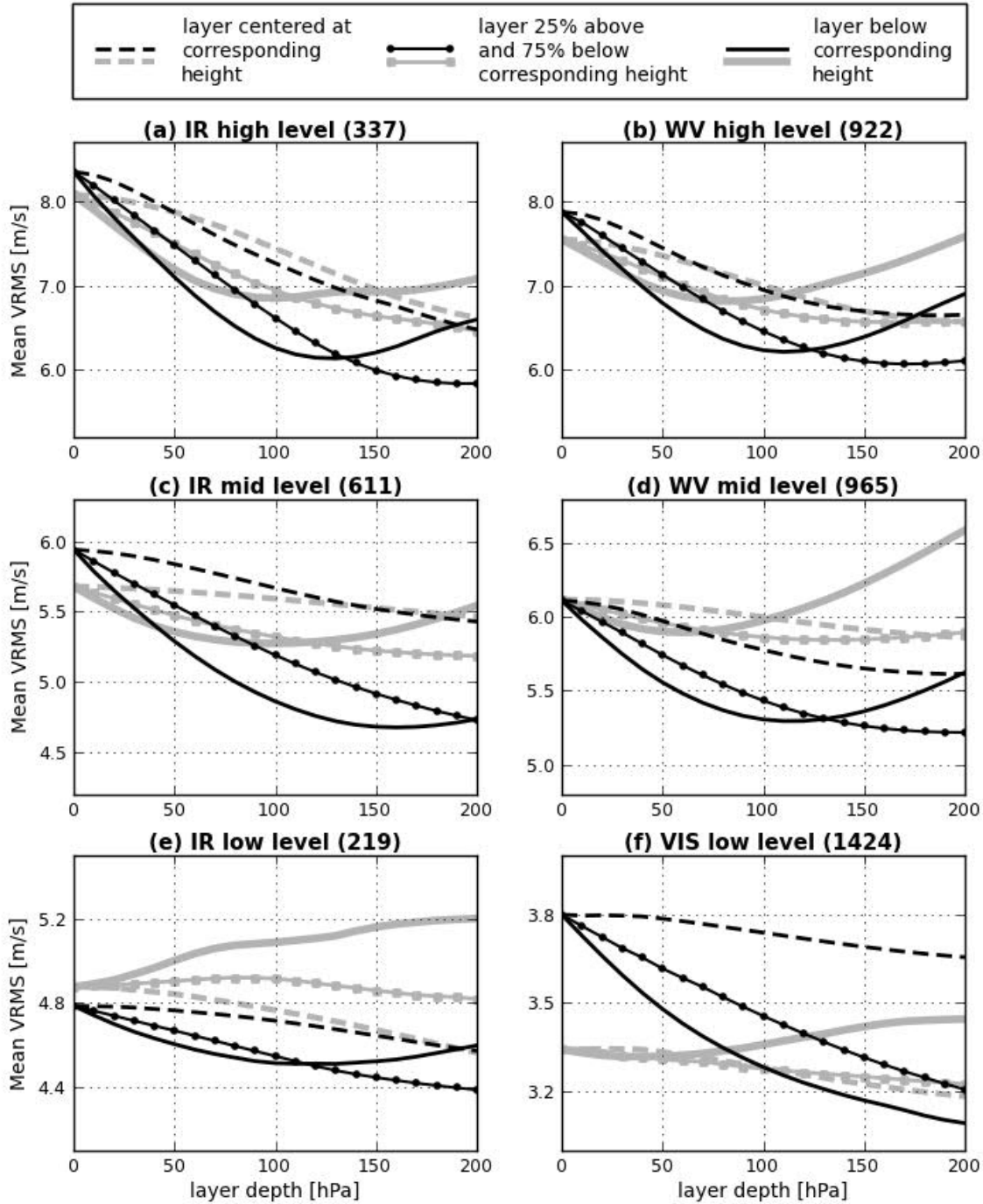


FIG 3. Mean VRMS differences between AMV winds and layer-averaged radiosonde winds for (a) high level IR-AMVs, (b) high level WV-AMVs, (c) mid level IR-AMVs, (d) mid level WV-AMVs, (e) low level IR-AMVs and (f) low level VIS-AMVs. Numbers in brackets are AMV counts for the respective graph. Grey lines represent layers relative to the original AMV pressure height, black lines relative to the lidar cloud top height. The three different layer positions are indicated by different line styles (cf. legend).

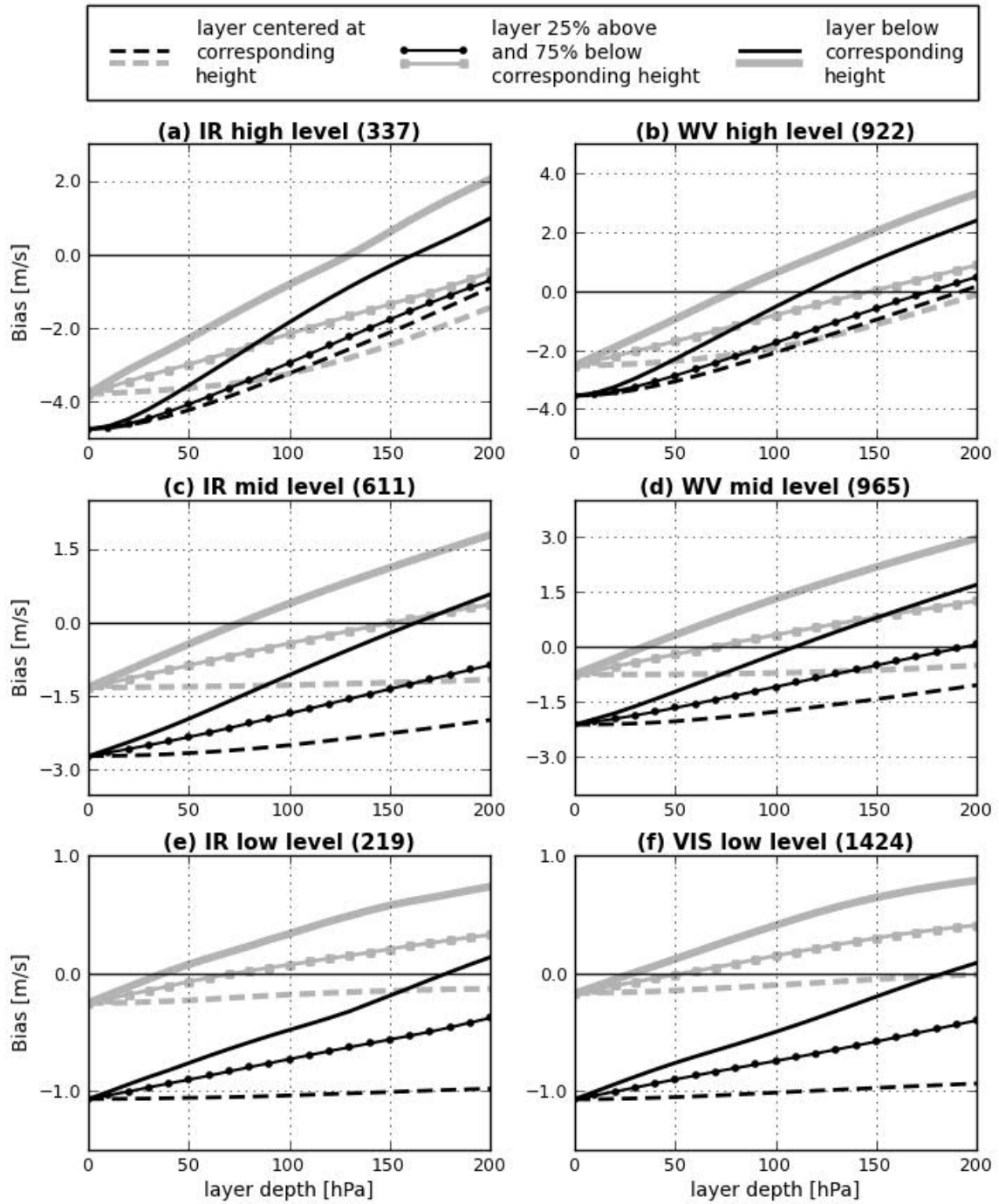


FIG. 4. As in Fig. 3 but for wind speed bias. Grey lines represent layers relative to the original AMV pressure height, black lines relative to the lidar cloud top height.

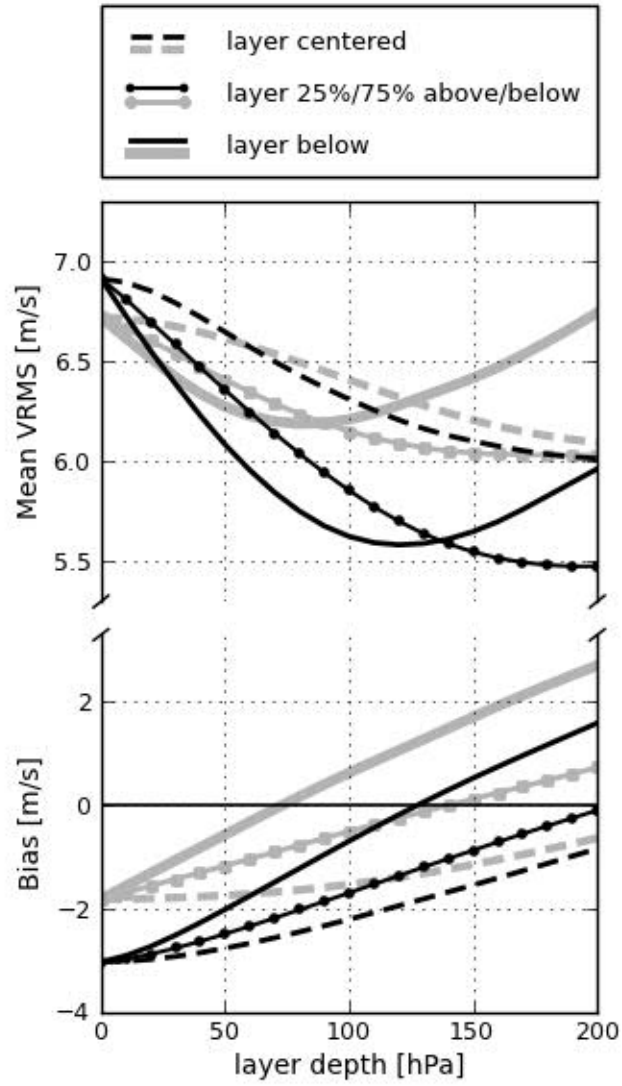


FIG. 5. Mean VRMS and wind speed bias of differences between AMV winds and layer-averaged radiosonde winds for upper level AMVs above 700 hPa (IR and WV combined). Altogether, 2835 AMVs are used (948 IR and 1887 WV). Grey lines represent layers relative to the original AMV pressure height, black lines relative to the lidar cloud top height. Note that the scales for bias and mean VRMS values are different.

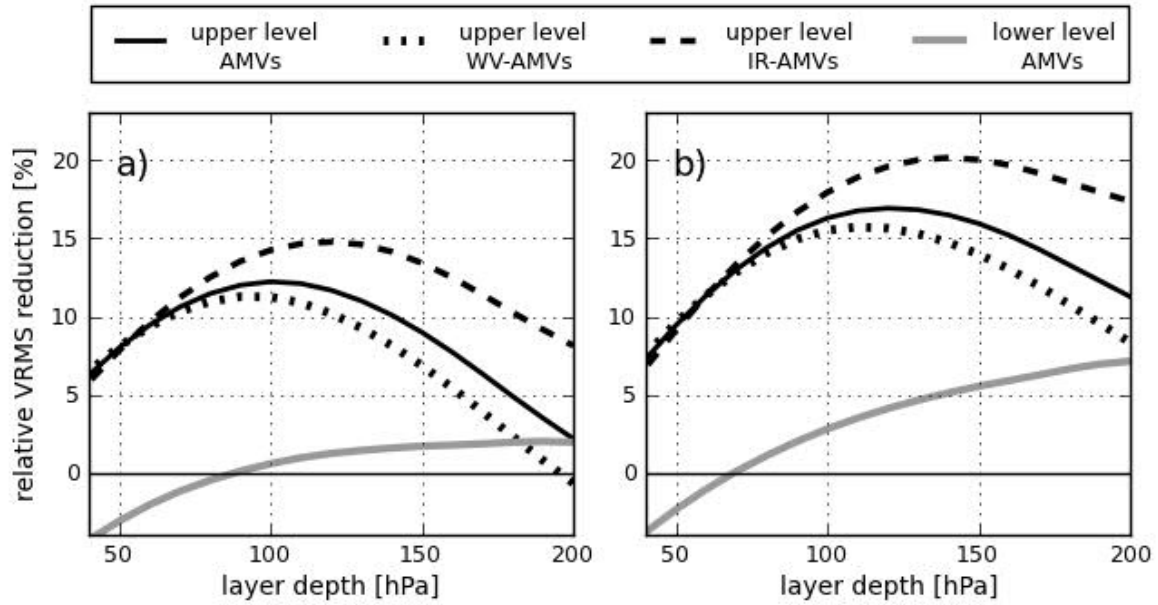


FIG. 6. Relative reduction of VRMS differences between AMV and radiosonde winds for assigning AMVs to layers below the lidar cloud tops instead of (a) layers of the same depth centered at the original AMV heights and (b) the discrete original AMV heights. Upper level AMVs above 700 hPa (black solid line) are additionally divided into upper level WV-AMVs (black dotted) and upper level IR-AMVs (black dashed). The grey solid line represents results for lower level AMVs (≥ 700 hPa).

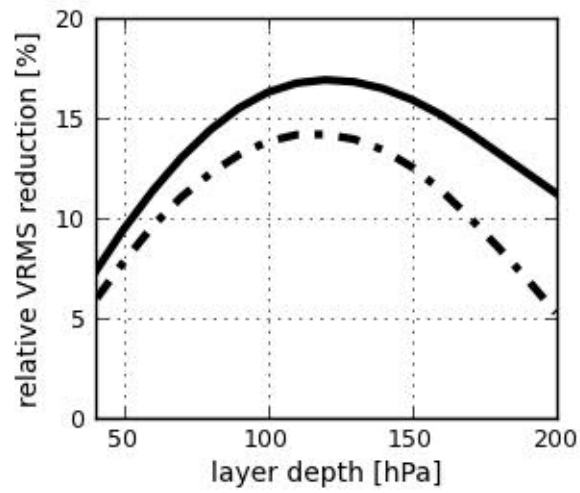


FIG. 7. Relative reduction of VRMS differences between AMV and radiosonde winds for assigning AMVs to layers below the lidar cloud tops (solid line) and to the respective mean pressure levels of that layer below lidar cloud tops (dashed-dotted line) instead of the discrete original AMV heights.

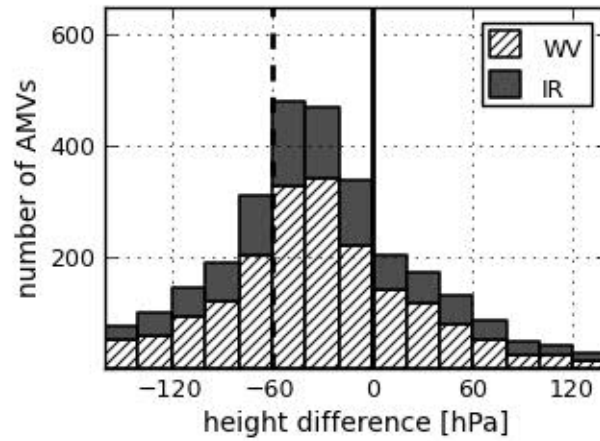


FIG. 8. Histogram of height differences (hPa) between the original AMV pressure height and the mean pressure of the corresponding 120 hPa layers below the lidar cloud top for upper level AMVs above 700 hPa (1887 WV-AMVs and 948 IR-AMVs). The dashed vertical line corresponds to the pressure height of the lidar cloud top.

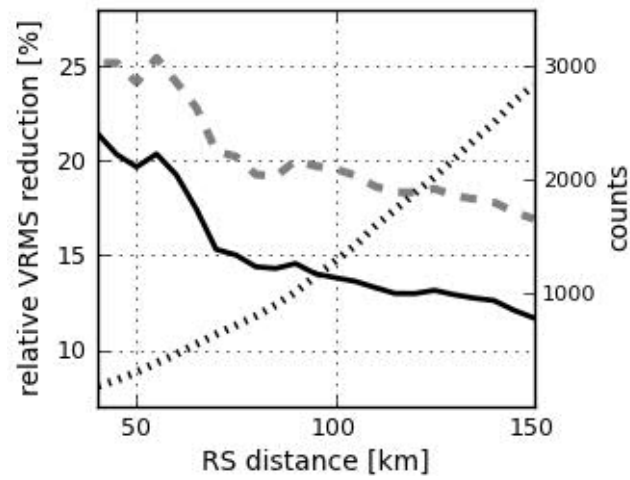


FIG. 9. Relative VRMS reduction of differences between AMV and radiosonde winds as a function of their horizontal distance for assigning AMVs to 120 hPa layers below the lidar cloud tops instead of layers centered at the original AMV heights (solid line) and the original discrete AMV heights (dashed line). The dotted line corresponds to the y-axis-label on the right and shows the sample size.